Available online at www.sciencedirect.com

SciVerse ScienceDirect

Geochimica et Cosmochimica Acta 84 (2012) 369–379

Geochimica et Cosmochimica Acta

www.elsevier.com/locate/gca

Hydrothermal fluids, argon isotopes and mineralization ages of the Fankou Pb–Zn deposit in south China: Insights from sphalerite $^{40}Ar/^{39}Ar$ progressive crushing

Ying-De Jiang [a,b], Hua-Ning Qiu [a,*], Yi-Gang Xu [a]

[a] State Key Laboratory of Isotope Geochemistry, Guangzhou Institute of Geochemistry, Chinese Academy of Sciences, Guangzhou 510640, China
[b] Department of Earth Sciences, The University of Hong Kong, Pokfulam Road, Hong Kong, China

Received 28 April 2011; accepted in revised form 26 January 2012; available online 9 February 2012

Abstract

Hydrothermal fluid geochemistry and mineralization timing are two important factors in the genesis of a hydrothermal deposit. $^{40}Ar/^{39}Ar$ analyses of fluid inclusions not only provide time constraints for the mineralization but also help to clarify the K–Ca–Cl–Ar characteristics for the ore-forming fluids. In this study, six sphalerite samples collected from the Fankou lead–zinc sulfide deposit are investigated by $^{40}Ar/^{39}Ar$ *in vacuo* crushing. Gases liberated from the early and late crushing steps exhibit distinct Ar isotopic compositions and $^{40}Ar/^{39}Ar$ apparent ages. Argon released in the early steps has much higher ^{40}Ar and $^{38}Ar_{Cl}$ and lower $^{37}Ar_{Ca}$ contents than those in the late steps. The significant excess Ar ($^{40}Ar_E$) extracted in the early crushing steps shows a strong correlation with $^{38}Ar_{Cl}$ with very high $^{40}Ar_E/^{38}Ar_{Cl}$ ratios. In contrast, those of the late steps mainly consist of atmospheric Ar and K-correlated radiogenic Ar with a constant $^{40}Ar_R/^{39}Ar_K$ ratio and the atmospheric initial $^{40}Ar/^{36}Ar$ ratio. As a result, all samples yield similar declining age spectra: the fore segments with anomalously old apparent ages decline quickly in the early crushing steps and the rear ones are flat with concordant apparent ages in the late crushing steps. The data points of the early steps define linear correlations in plots of $^{40}Ar_{NA}/^{39}Ar_K$ vs. $^{38}Ar_{Cl}/^{39}Ar_K$ and $^{38}Ar_{Cl}/^{40}Ar_{NA}$ vs. $^{39}Ar_K/^{40}Ar_{NA}$ (NA for non-atmospheric) and most yield ages of 240–230 Ma. On the other hand, the data of the late steps always construct well-defined isochrons in the plots of $^{36}Ar_A/^{40}Ar_{NA}$ vs. $^{39}Ar_K/^{40}Ar_{NA}$ with consistent ages of ~300 Ma. We interpret that gases released in the early steps were from the secondary fluid inclusions (SFIs) due to their distribution characteristics along cracks leading to be easily extracted, and those released in the later steps represented the contribution of the primary fluid inclusions (PFIs). The initial $^{40}Ar/^{36}Ar$ ratios of SFIs, much higher than the modern atmospheric ratio, suggest that their fluids were most likely from deep sources. However, these ratios of PFIs, close to the modern atmospheric ratio, might imply that the ore-forming fluids were mainly meteoric. Accordingly, our results show that a major lead–zinc mineralization occurred at about 300 Ma and a subsequent hydrothermal interruption at 240–230 Ma. The sphalerite $^{40}Ar/^{39}Ar$ crushing results suggest that the ore-forming fluid might strongly interact with the sedimentary rocks resulting in the enrichment of ore deposit.

* Corresponding author. Address: State Key Laboratory of Isotope Geochemistry, Guangzhou Institute of Geochemistry, Chinese Academy of Sciences, P.O. Box 1131, Guangzhou 510640, China. Tel./fax: +86 20 85290125.
E-mail address: qiuhn@gig.ac.cn (H.-N. Qiu).

0016-7037/$ - see front matter © 2012 Elsevier Ltd. All rights reserved.
doi:10.1016/j.gca.2012.01.044

1. INTRODUCTION

The mineralization age and fluid origin are essential data to better understand the genesis of a hydrothermal deposit. In recent years, $^{40}Ar/^{39}Ar$ progressive crushing *in vacuo* for the fluid inclusions in minerals has opened up a new way of dating hydrothermal deposits (Kelley et al., 1986; Turner, 1988; Qiu and Dai, 1989; Burgess et al., 1992; Turner and Bannon, 1992; Turner and Wang, 1992; McKee et al., 1993; Qiu, 1996; Kendrick et al., 2001; Qiu et al., 2002; Qiu and Wijbrans, 2006, 2008). Except for determining the radio-isotopic ages, this technique has also been extended to analyze the abundances of K, Cl and Ca and their correlations in the fluid inclusions because of their derived argon isotopes of $^{39}Ar_K$, $^{38}Ar_{Cl}$ and $^{37}Ar_{Ca}$ during the irradiation, which is very helpful to identify the fluid sources (Kelley et al., 1986; Turner and Bannon, 1992; Turner and Wang, 1992; Kendrick et al., 2001; Qiu et al., 2002). In addition, this technique has been suggested to be able to distinguish gases from different reservoirs (Qiu and Wijbrans, 2006, 2008).

Our preliminary test of sphalerite by $^{40}Ar/^{39}Ar$ crushing has shown the possibility of dating sulfide mineralization directly and the potential of distinguishing the primary and secondary fluid inclusions (see Qiu and Jiang, 2007). This successive study further investigates the potential of sphalerite for direct dating hydrothermal sulfide deposits by $^{40}Ar/^{39}Ar$ progressive crushing, the degassing patterns and the K–Ca–Cl elemental correlations within the fluid inclusions, which will help us to better understand the genesis of the ore deposit.

2. GEOLOGICAL BACKGROUND AND SAMPLE DESCRIPTIONS

The Fankou super-large lead–zinc deposit occurs in the Middle–Upper Devonian and Lower Carboniferous carbonate, shale and argillaceous carbonate formations (Song, 1984) in northern Guangdong Province, southern China. The ore bodies are usually stratiform, lentiform and irregular in shape. The stratiform ones distribute conformably with the sedimentary host rocks, and the lentiform and irregular ones are spatially associated with the fault systems (see Fig. 1). The ore minerals include sphalerite and galena, associated with vein minerals of pyrite, calcite and dolomite.

In the present study, six ore specimens (04FK-01, 03, 05, 07, 14 and 18) were collected from different mining levels of Middle–Upper Devonian and pure sphalerite aggregates were separated from each of them for individual $^{40}Ar/^{39}Ar$ isotopic analyses by *in vacuo* crushing.

Basically, there are two kinds of fluid inclusions recognized in the sphalerite grains. The primary fluid inclusions (PFIs) in sphalerite are elliptical, round and xenomorphic in shape, mainly ranging from 1 to 5 μm in size, and are as randomly distributed (see Fig. 2). The secondary fluid inclusions (SFIs) are usually larger than 5 μm and commonly distributed in trails along the microcracks (e.g. Fig. 2b). The larger inclusions mostly contain both liquid

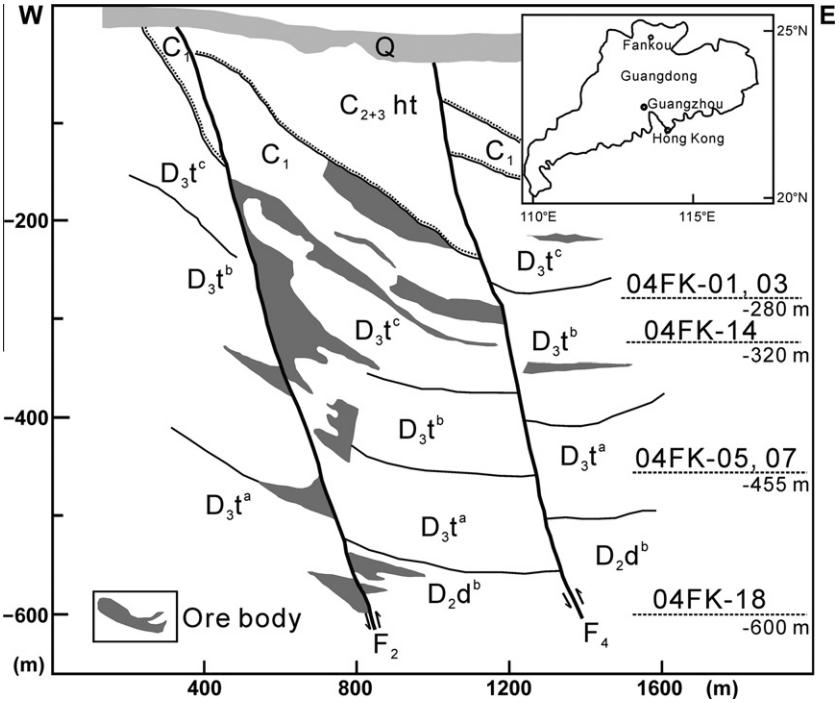

Fig. 1. Simplified cross-section of the Fankou Pb–Zn Deposit (modified from Zhang, 2001), showing stratigraphy of ores and sampling sites. The ore bodies are usually stratiform, lentiform and irregular in shape and are spatially associated with faults. Q-Quaternary sediment; C_{2+3}ht-carbonate of the Middle–Upper Carboniferous Hutian Group; C_1-argillaceous carbonates of Lower Carboniferous; D_3t^c, D_3t^b, D_3t^a-carbonate of the Upper Devonian Tianziling Formation; D_2d^b-carbonate of the upper subformation of the Middle Devonian Donggangling Formation; F-Fault. Inset figure shows the location of Fankou Mine.

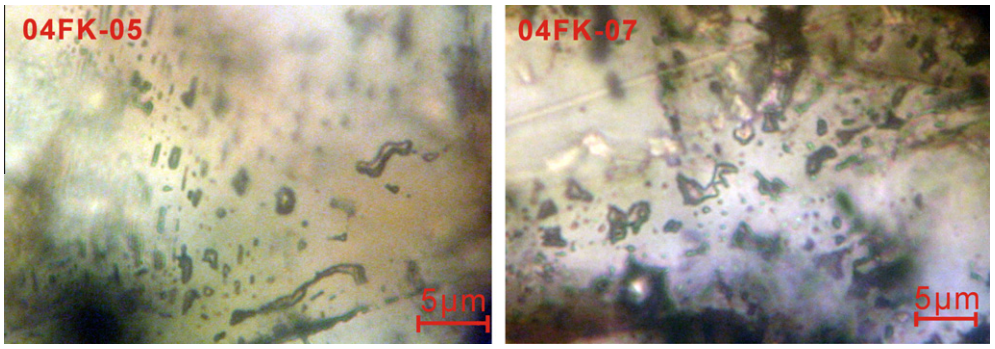

Fig. 2. Photomicrographs of sphalerite samples showing a great abundant of primary fluid inclusions which are randomly distributed with elliptical and round shapes and 1–5 μm sizes. Secondary fluid inclusions are locally present, which have relatively larger sizes and usually distributed in trails along the microcracks.

and gaseous CO_2 phases. However, in the small ones (<1 μm) this distribution is not observed.

3. ANALYTICAL METHODS

The specimens were individually crushed in a stainless steel mortar and then sieved. The sieved fractions of 30–60 mesh (0.50–0.25 mm) in size were cleaned with deionized water in an ultrasonic bath and then dried in an oven at 80 °C. Sphalerite grains were carefully separated by hand picking under a binocular microscope to obtain single minerals of 99% purity.

The sphalerite samples of ~50 mg each were packed up for neutron irradiation together with the monitor standard DRA1 (sanidine with an age of 25.26 ± 0.07 Ma, modified from Wijbrans et al., 1995 to the calibration recommended by Renne et al., 1998). The monitor DRA1 splits were inserted between every five samples and both ends of the sample tubes. A curve (or line) of *J*-value vs. height was obtained on the DRA1 splits for each tube, and then the *J*-value of each sample was calculated by interpolation from the curve. The *J*-value uncertainty of 0.15% (1σ) was incorporated in the age uncertainty. The experiments were carried out on an improved crusher that was described in detail in our previous papers (Qiu and Jiang, 2007; Qiu and Wijbrans, 2008). Prior to analysis, the whole apparatus was baked out at 150 °C using a heating tape and the crusher was heated at 170 °C with a furnace for *ca.* 10 h in order to reduce the blanks. Samples were crushed by repeatedly lifting and dropping the pestle through a ~5 cm vertical height using an external electric magnet. The frequency was controlled at 2.5 Hz by an adjustable repeating-timer-relay. The impact number for each extraction was recorded on a digital counter, and increased to maintain an argon beam intensity level sufficiently high for measurement. The crushing experiments were continued until the argon level diminished significantly, indicating exhaustion of the source of argon in the fluid inclusions. The released gases were purified for 5–8 min by two SAES-NP10® getters at room temperature and ~400 °C, respectively. Argon isotopes were analyzed with a GVI-5400® mass spectrometer in our laboratory. A blank experiment was run after every four or five crushing steps. The blanks were: ^{36}Ar (0.002–0.018) mV, ^{37}Ar (0.0001–0.0009) mV, ^{38}Ar (0.0004–0.003) mV, ^{39}Ar (0.002–0.017) mV and ^{40}Ar (0.6–5.4) mV. The ^{39}Ar signals of the crushing samples were usually hundreds to thousands of times as the ^{39}Ar blanks.

4. RESULTS

The $^{40}Ar/^{39}Ar$ data were corrected, calculated and plotted using the ArArCALC software package (Koppers, 2002). Analytical, internal and external errors were calculated on the error propagations of all input parameters, analytical data and applied corrections. All the results are summarized and saved in an Excel workbook available for inspection in electronic annex Appendix Table A1. The argon isotope intensities and their uncertainties were expressed throughout in volts. Correction factors for interfering argon isotopes derived from Ca and K are: $(^{39}Ar/^{37}Ar)_{Ca} = 8.984 \times 10^{-4}$, $(^{36}Ar/^{37}Ar)_{Ca} = 2.673 \times 10^{-4}$ and $(^{40}Ar/^{39}Ar)_{K} = 5.97 \times 10^{-3}$. Due to the lack of the Cl concentration of the monitor DRA1, we use the neutron-induced argon isotopes of $^{37}Ar_{Ca}$, $^{38}Ar_{Cl}$ and $^{39}Ar_{K}$ to represent Ca, Cl and K, respectively. The degassing patterns of argon isotopes are shown in Fig. 3. The correlations amongst Ca-, Cl- and K-derived argon isotopic ratios are also listed in electronic annex Appendix Table A1 and illustrated in Figs. 4–6. The $^{40}Ar/^{39}Ar$ dating results are presented in age spectra (Fig. 7) and inverse isochron diagrams of $^{36}Ar/^{40}Ar$ vs. $^{39}Ar/^{40}Ar$ (Fig. 8). All the errors are in 1σ in the text and figures.

4.1. Correlations amongst Ca-, Cl- and K-derived Ar isotopes

Five argon isotopes exist in $^{40}Ar/^{39}Ar$ analyses: ^{36}Ar, ^{37}Ar, ^{38}Ar, ^{39}Ar and ^{40}Ar. ^{40}Ar is always a mixture from several different sources (Kelley et al., 1986; Turner and Bannon, 1992; Turner and Wang, 1992; Qiu and Wijbrans, 2006, 2008), including: (1) atmospheric $^{40}Ar_A$ accompanied by $^{36}Ar_A$ with a $^{40}Ar/^{36}Ar$ ratio of 295.5, dissolved in aqueous fluid inclusions, (2) radiogenic $^{40}Ar_R$ produced by *in situ* K decay, and (3) parentless excess ^{40}Ar (denoted as $^{40}Ar_E$), representing ^{40}Ar degassed or leached from the crust. Here $^{40}Ar_{NA}$ is introduced to express the ^{40}Ar relic after applying interfering and atmospheric argon

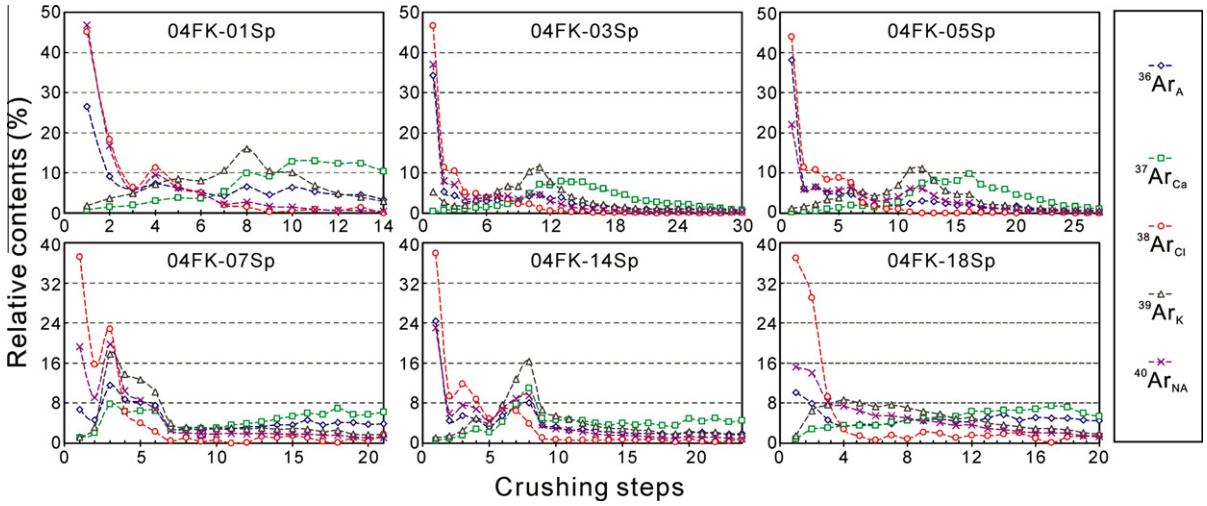

Fig. 3. Relative release of argon isotopes by sphalerite *in vacuo* crushing experiments showing diverse degassing profiles for different components.

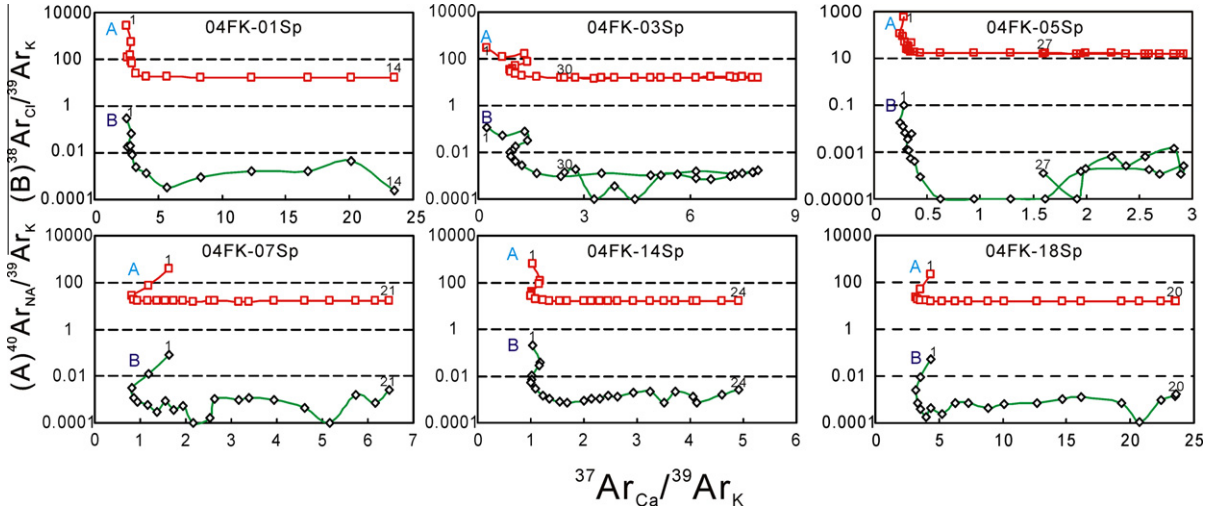

Fig. 4. Composite plots of the correlations amongst Cl-, K-, Ca-derived argon isotopes based on the $^{40}Ar/^{39}Ar$ data of sphalerites by *in vacuo* crushing. Series (A) represents the data set of $^{40}Ar_{NA}/^{39}Ar_K$ and series (B) stands for the data set of $^{38}Ar_{Cl}/^{39}Ar_K$. First and last crushing steps are numbered to show the crushing sequence. See text for further information.

corrections (NA: non-atmospheric), that is, including $^{40}Ar_R$ and $^{40}Ar_E$.

The argon release patterns of sphalerite by crushing indicate that very large amounts of $^{40}Ar_{NA}$ and chlorine-derived $^{38}Ar_{Cl}$ were released in the early crushing steps (see Fig. 3 and Table A1). Most calcium-derived $^{37}Ar_{Ca}$ and potassium-derived $^{39}Ar_K$ were liberated subsequently with peaks at the middle crushing steps. The atmospheric $^{36}Ar_A$ component steadily decreases with continued crushing. For example, sample 04FK-03Sp underwent a total of 10,410 pestle drops in 30 crushing steps. 72.1% $^{40}Ar_{NA}$ and 90.8% $^{38}Ar_{Cl}$ were released by the first 430 pestle drops. However, 43.0% $^{39}Ar_K$ and 42.5% $^{37}Ar_{Ca}$ were extracted from steps 10 to 15. The $^{36}Ar_A$ signals decreased from 1.31 mV at the first step to 0.03 mV at the last step.

Several representations are employed here to illustrate various features of the argon isotopic data. The gases of the early steps are characterized by relatively high $^{40}Ar_{NA}/^{39}Ar_K$, $^{38}Ar_{Cl}/^{39}Ar_K$ but low $^{37}Ar_{Ca}/^{39}Ar_K$ ratios in comparison with those of the late steps (Table A1). These features are distinctly displayed on the 2-D plots of $^{40}Ar_{NA}/^{39}Ar_K$ vs. $^{37}Ar_{Ca}/^{39}Ar_K$ (Fig. 4, curves A) and $^{38}Ar_{Cl}/^{39}Ar_K$ vs. $^{37}Ar_{Ca}/^{39}Ar_K$ (Fig. 4, curves B). As the crushing experiments progressed, the $^{40}Ar_{NA}/^{39}Ar_K$ ratios decreased markedly in the early steps and then remained constant in the late steps. The $^{38}Ar_{Cl}/^{39}Ar_K$ ratios have the same declining trends with the $^{40}Ar_{NA}/^{39}Ar_K$ ratios but with the extremely low $^{38}Ar_{Cl}$ signals (less than 3×10^{-3} mV) in the late steps. The $^{37}Ar_{Ca}/^{39}Ar_K$ ratios, however, usually rise step by step.

On the plots of $^{40}Ar_{NA}/^{39}Ar_K$ against $^{38}Ar_{Cl}/^{39}Ar_K$ (Fig. 5), the data points of the early steps show good linear correlations with $^{40}Ar_{NA}/^{39}Ar_K$ intercepts of 13.4–12.0, corresponding to ages of 249–227 Ma. These ages based

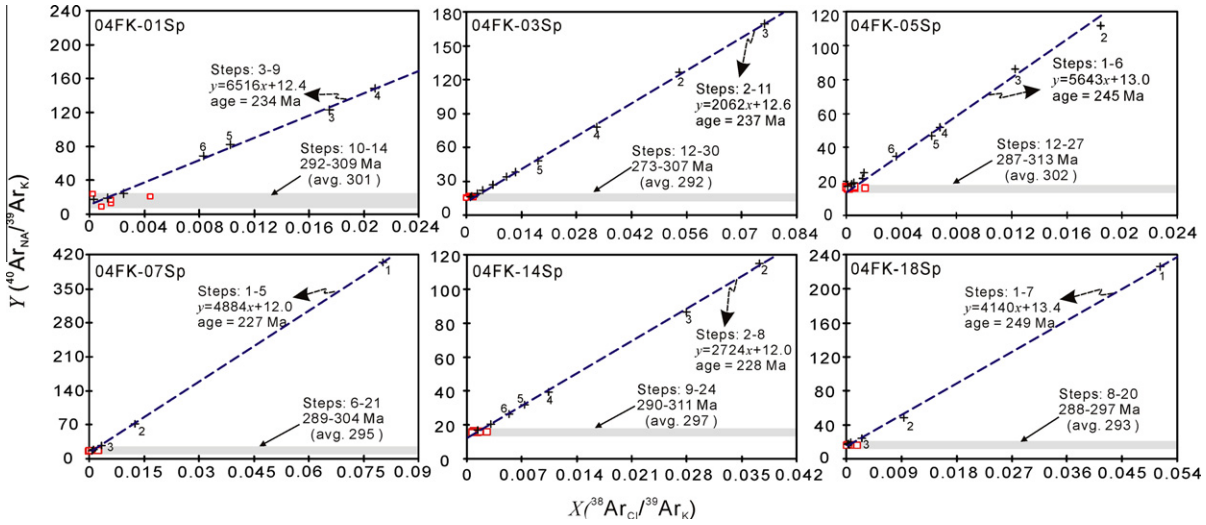

Fig. 5. Plots of the correlation between $^{40}Ar_{NA}/^{39}Ar_K$ and $^{38}Ar_{Cl}/^{39}Ar_K$ for *in vacuo* crushing data from sphalerites. $^{40}Ar_{NA}$ shows strong correlation with $^{38}Ar_{Cl}$ in the early crushing steps. Crushing steps were numbered to show the sequence of crushing. Some initial crushing steps with extremely high $^{40}Ar_{NA}/^{39}Ar_K$ and $^{38}Ar_{Cl}/^{39}Ar_K$ values are not shown.

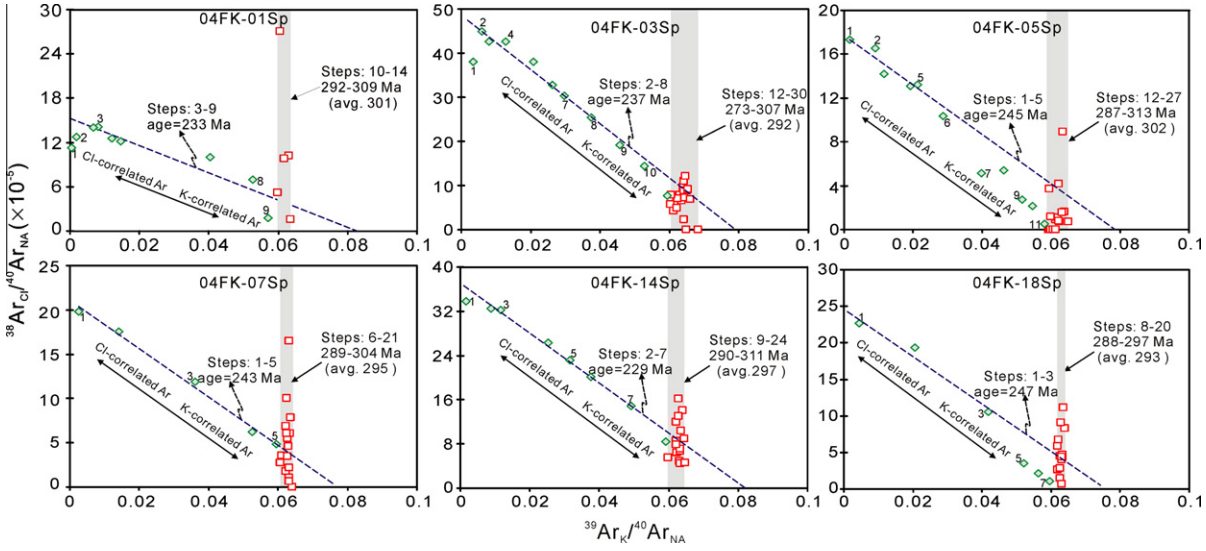

Fig. 6. Plots of $^{38}Ar_{Cl}/^{40}Ar_{NA}$ against $^{39}Ar_K/^{40}Ar_{NA}$ for individual crushing measurements on sphalerites. Early steps are numbered to show the crushing sequence.

on the data of the early crushing steps are interpreted as the contributions of the secondary fluid inclusions (SFIs), as discussed later. In contrast, the late crushing steps (open squares in Fig. 5) released extremely low $^{38}Ar_{Cl}$ without any correlation between $^{40}Ar_{NA}/^{39}Ar_K$ and $^{38}Ar_{Cl}/^{39}Ar_K$, but with constant $^{40}Ar_{NA}/^{39}Ar_K$ ratios close to the vertical axis. The average $^{40}Ar_{NA}/^{39}Ar_K$ ratios of the six samples are from 16.2 to 15.7, corresponding to ages from 302 to 292 Ma. These ages based on the data of the late crushing steps are interpreted as the contributions of the primary fluid inclusions (PFIs).

Unlike the $^{40}Ar_{NA}$ component, the $^{39}Ar_K$ has an inverse correlation with the $^{38}Ar_{Cl}$ based on the data of the early crushing steps (see Fig. 6). The $^{38}Ar_{Cl}/^{40}Ar_{NA}$ ratios gradually descend with the experimental process in the early steps until almost zero in the end, whilst the $^{39}Ar_K/^{40}Ar_{NA}$ ratios ascend monotonically in the beginning until constant values in the late steps. Excluding the most dispersed points, correlation lines between $^{38}Ar_{Cl}/^{40}Ar_{NA}$ and $^{39}Ar_K/^{40}Ar_{NA}$ are drawn for the early crushing steps with $^{39}Ar_K/^{40}Ar_{NA}$ intercepts of 0.0757–0.0834, corresponding to ages of 247–229 Ma. On the other hand, the late crushing steps yield concordant $^{39}Ar_K/^{40}Ar_{NA}$ ratios varying in very narrow ranges with wide $^{38}Ar_{Cl}/^{40}Ar_{NA}$ ratio changes (but mostly less than 0.0001), showing a distinctly different domain from that of the early steps. The concordant $^{39}Ar_K/^{40}Ar_{NA}$ ratios of 0.061–0.063 correspond to ages of 302–292 Ma.

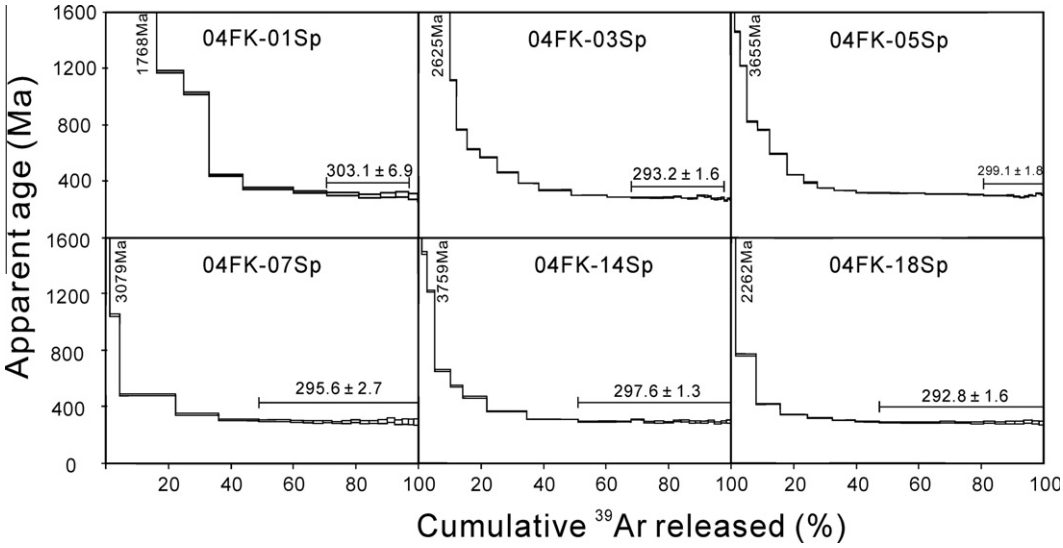

Fig. 7. $^{40}Ar/^{39}Ar$ age spectra of sphalerite samples by *in vacuo* crushing, showing consistent plateau ages.

4.2. $^{40}Ar/^{39}Ar$ plateau and isochron ages

All the six sphalerite samples yield similar $^{40}Ar/^{39}Ar$ age spectra. These begin with unreasonably old apparent ages during the first several steps, decrease remarkably during subsequent steps and finally form flat plateaus with plateau ages of 303.1 ± 6.9, 293.2 ± 1.6, 299.1 ± 1.8, 295.6 ± 2.7, 297.6 ± 1.3 and 292.8 ± 1.6 Ma, for samples 04FK-01Sp, 03Sp, 05Sp, 07Sp, 14Sp and 18Sp, respectively (see Fig. 7). On inverse isochron plots of $^{36}Ar/^{40}Ar$ vs. $^{39}Ar/^{40}Ar$, the data points corresponding the plateaus define isochrons with ages of 309.8 ± 31.8, 294.5 ± 8.7, 299.8 ± 6.0, 297.4 ± 7.9, 298.9 ± 5.4, and 293.7 ± 4.0 Ma, respectively (Fig. 8). The initial $^{40}Ar/^{36}Ar$ ratios of all isochrons are concordant and close to the modern atmospheric ratio of 295.5.

Another isochron is found for the data points of steps 2–6 of sample 04FK-05Sp with a young age of 231.5 ± 15.2 Ma and a relatively high $^{40}Ar/^{36}Ar$ initial ratio of 1031 ± 17 (Fig. 8c), indicating the existence of excess ^{40}Ar ($^{40}Ar_E$). Excluding the $^{40}Ar_E$ with this initial ratio for steps 2–6, produces a weighted mean age of 231.7 ± 6.1 Ma, agreeing with the isochron age.

5. DISCUSSION

5.1. Argon reservoirs liberated during progressive crushing

5.1.1. Chemical characteristics

Gases released from the early crushing steps have very high $^{40}Ar_{NA}$ concentrations as well as very high $^{40}Ar_{NA}/^{39}Ar_K$ ratios, resulting in anomalously old apparent ages, even older than the Earth's age. This reflects that the related gases contain a significant amount of $^{40}Ar_E$. This component is interpreted as Cl-correlated $^{40}Ar_E$ since it is strongly correlated with the $^{38}Ar_{Cl}$ (Fig. 5). In comparison, gases released from the late crushing steps have relatively low $^{40}Ar_{NA}$ but high $^{37}Ar_{Ca}$ and extremely low $^{38}Ar_{Cl}$ signals. The inferred initial $^{40}Ar/^{36}Ar$ ratios for these later steps are close to that of modern atmosphere, indicating exhaustion of $^{40}Ar_E$. The noticeable transition from the early crushing stages to later ones in almost all representations as illustrated above probably suggests that different reservoirs were contributing to the degassing during early and later crushing steps, respectively. In general, gases released from the late crushing steps have relatively simple isotopic systematics compared to early steps, as evidenced by their identical $^{40}Ar_{NA}/^{39}Ar_K$ ratios and well-defined isochrons and age plateaus.

5.1.2. Possible argon reservoirs contributing to degassing

Ar isotopic components including radiogenic Ar and excess Ar may be preserved in both solid and liquid phases. It has been suggested that those in liquid phase, like fluid inclusions, could be easily extracted by *in vacuo* crushing (Kelley et al., 1986; Turner, 1988; Turner and Bannon, 1992; Turner and Wang, 1992). This idea has been strongly supported by recent $^{40}Ar/^{39}Ar$ dating of some hydrothermal minerals (Qiu, 1996; Kendrick et al., 2001; Qiu et al., 2002; Qiu and Wijbrans, 2006, 2008). Argon hosted in the solid phase, i.e., locked within the crystal lattice, except when residing along microcracks and/or on mineral interfaces (if any), however, has been suggested to be more retentive (Kelley et al., 1986; Turner and Wang, 1992; Qiu et al., 2002; Qiu and Wijbrans, 2008). These studies have further documented that argon trapped in the solid phase can be effectively extracted by heating. It is noteworthy that even by applying sufficient crushing on pure K-rich mica at 400 °C and 100–200 MPa (Dunlap and Kronenberg, 2001), the level of argon lost is likely to be insignificant, similar to the limit of resolution of typical dating studies, although Kendrick and Phillips (2009), while working on scapolite found a more significant contribution of what they argued to be lattice hosted argon while crushing. Moreover, it has been well documented that chemical components such as K, Ca, Cl and $^{40}Ar_E$ and their ratios in fluid

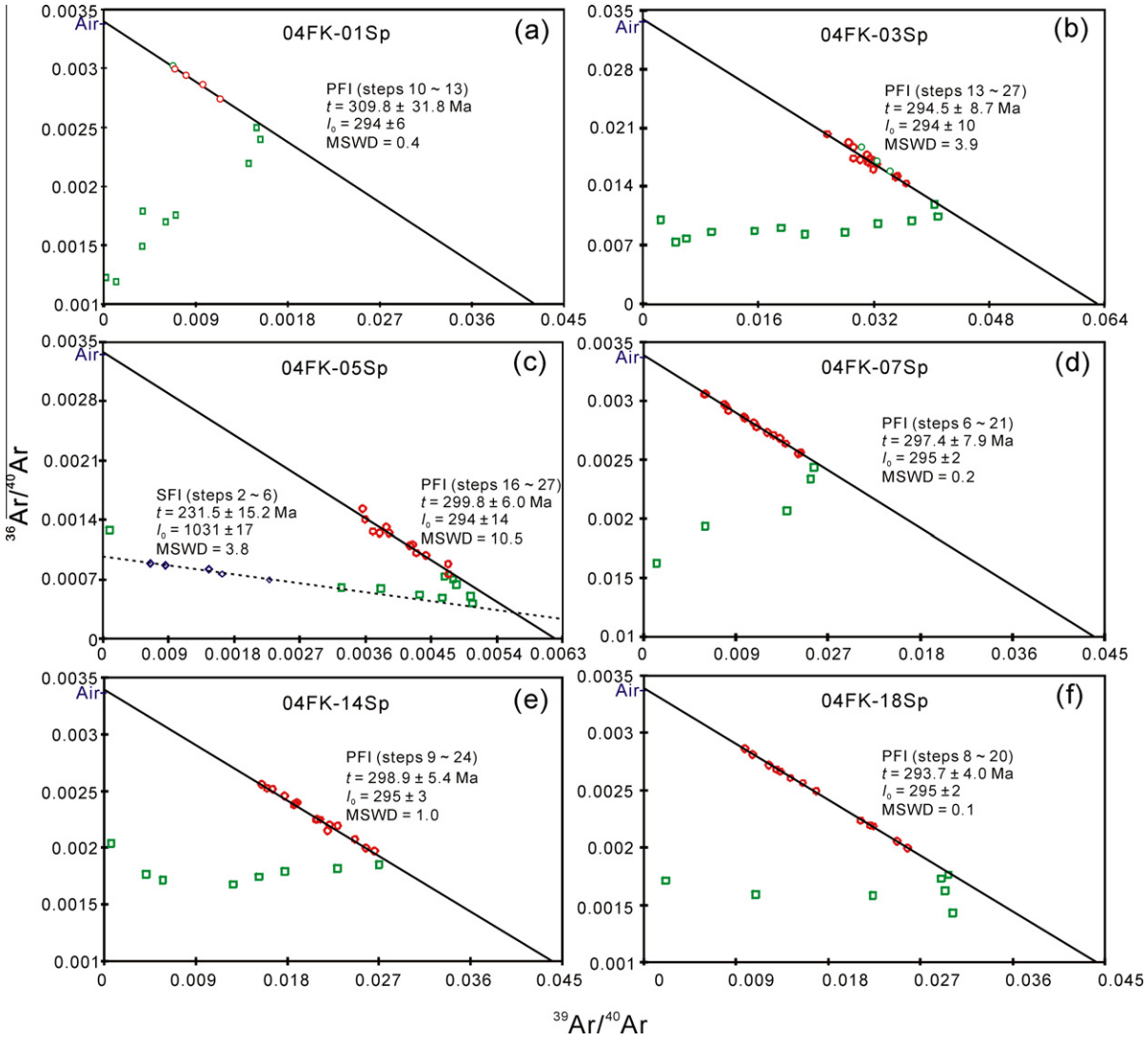

Fig. 8. $^{40}Ar/^{39}Ar$ inverse isochron lines for sphalerites obtained from *in vacuo* crushing. Data points represent crushing steps defining the isochrons and corresponding age plateaus. ^{40}Ar was calculated by applying a standard 'air correction' assuming $^{40}Ar/^{36}Ar = 295.5$.

inclusions (by crushing) can be remarkably different from those of the solid phase (by heating crushed powders), although in some cases they yield identical ages (Turner and Bannon, 1992; Turner and Wang, 1992; Qiu, 1996; Qiu et al., 2002; Kendrick et al., 2006a,b; Qiu and Wijbrans, 2006, 2008, 2009; Qiu and Jiang, 2007; Kendrick and Phillips, 2009).

5.1.2.1. SFIs in the early crushing steps. The correlation between $^{40}Ar_{NA}$ and $^{38}Ar_{Cl}$ has been proposed as an indicator to monitor the degassing of fluid inclusions (Turner and Bannon, 1992; Turner and Wang, 1992), since the entrapment of Cl in aqueous fluids always leads to the correlation between neutron-induced $^{38}Ar_{Cl}$ and naturally occurring argon dissolved in the fluids. The strong correlation between $^{40}Ar_{NA}$ and $^{38}Ar_{Cl}$ in the early crushing steps thus clearly indicates a fluids-related origin for the extracted gases. As mentioned before, due to their relatively large volume and distribution characteristics along cracks, the SFIs can be easily extracted during the early crushing steps. This idea has been well documented by $^{40}Ar/^{39}Ar$ crushing of hydrothermal minerals (Qiu et al., 2002; Kendrick et al., 2006a; Qiu and Wijbrans, 2006, 2008; Qiu and Jiang, 2007). We note that the data points of some initial one or two crushing steps (e.g. 04FK-01Sp, 03Sp and 14Sp) significantly depart away from those of the subsequent crushing steps (see Figs. 5 and 6). This could be due to some excess argon within the microcracks and mineral interfaces being liberated.

5.1.2.2. PFIs in the late crushing steps. Because primary fluid inclusions (PFIs) are smaller in size than SFIs and they are more isolated and randomly distributed in host crystals, it should require more impacts to extract them. For the late crushing steps, the homogeneous compositions, consistent $^{40}Ar_{NA}/^{39}Ar_K$ ratios and well-defined isochrons suggest that a unique reservoir dominates the degassing. It is noteworthy that this reservoir dominated the degassing relatively early in the crushing process (less than 800 strokes

in the case of sample 04FK-14Sp, Table A1). It seems unlikely that such a small number of strokes are enough to remove all fluid inclusions and only leave the solid phase argon to contribute to the degassing during late stages of crushing. We therefore suggest that gases released in these late steps represent the contribution from the PFIs.

5.1.2.3. Mixing of SFIs and PFIs in the middle steps. Since the SFIs and PFIs are taken as the gas contributors respectively in the early and late crushing steps, the gas compositions in the middle steps should represent the mixtures with different proportions of the SFI and PFI end member phases. This explains why data points corresponding to the middle crushing stage commonly scatter between those of the early and late stages.

5.1.3. An example of the gas release processed by crushing

Sample 04FK-05Sp is a typical example. Nearly 53% of $^{40}Ar_{NA}$ and 91% of $^{38}Ar_{Cl}$ are contributed from the earliest 6 crushing steps and only 10% and 2%, respectively are from the last 12 steps (No. 16–27). The $^{37}Ar_{Ca}$, however, released only 6% from the earliest 6 crushing steps and 50% from the last 12 steps. The data set is easily subdivided into different groups as illustrated above. This is further illustrated by the inverse isochron plot (Fig. 8c). Steps 2–6 define an isochron with an age of 231.5 ± 15.2 Ma and initial $^{40}Ar/^{36}Ar$ ratio of 1031 ± 17. Steps 16–27 construct another isochron with an age of 299.8 ± 6.0 Ma and initial $^{40}Ar/^{36}Ar$ ratio of 294 ± 14. However, the middle steps 7–15 scatter between the two isochrons without a linear relationship, suggesting the mixing of the SFIs and PFIs in different proportions.

In conclusion, the gases in the early and late crushing steps have quite different argon components. Early releases are rich in $^{40}Ar_E$ and $^{38}Ar_{Cl}$, and late ones are poor in $^{40}Ar_E$ and $^{38}Ar_{Cl}$ but rich in $^{37}Ar_{Ca}$. We interpret the gases in the early steps as contributions from SFIs as well as microcracks (if any), those in the late steps from PFIs, and those in the middle steps mixing both SFIs and PFIs. The results indicate that the SFIs contain significant Cl-correlated excess argon ($^{40}Ar_E$) but the PFIs are free of excess argon.

5.2. Age significances and fluid origins

5.2.1. Age significances

The SFIs are easily extracted during the early crushing steps. Due to mixing of PFIs, it is difficult to obtain an isochron for the SFIs on the inverse isochron plot of $^{36}Ar/^{40}Ar$ vs. $^{39}Ar/^{40}Ar$, although now have three successful cases of samples 04FK-05Sp (this study, Fig. 8c), 04FK-02Sp and 04FK-11Sp (Qiu and Jiang, 2007) with quite concordant ages of 231–235 Ma. However, it is very interesting that we can obtain significant SFI age information from the $^{38}Ar_{Cl}$-correlated plots based on both plots of $^{40}Ar_{NA}/^{39}Ar_K$ vs. $^{38}Ar_{Cl}/^{39}Ar_K$ (Fig. 5) and $^{38}Ar_{Cl}/^{40}Ar_{NA}$–$^{39}Ar_K$–$^{38}Ar_{Cl}$ provide another potential approach for attaining the SFI's ages in spite of the presence of excess ^{40}Ar. The dominant SFI ages of 230–240 Ma indicate that a secondary fluid perturbation, possibly due to a post-mineralization hydrothermal activity, occurred in the Middle Triassic.

In the late crushing steps, the PFIs absolutely dominate the gas contributions, and yield concordant ages of 294–300 Ma for all six samples (see Figs. 5–8). We interpret this age to represent the timing of sulfide mineralization. According to our new age results, the main mineralization in the Fankou Pb–Zn deposit took place in Early Permian, quite different from the current estimates based on the wide Late Jurassic W-Sn mineralization in the adjacent area of South China (Mao et al., 2006, 2007).

5.2.2. Fluids origin constraints

It has been commonly accepted that the Ar-isotopic compositions of fluid inclusions may provide conclusive constraints on fluid origins (Kelley et al., 1986; Turner and Bannon, 1992). Compared to the SFIs, the PFIs have lower $^{38}Ar_{Cl}$ but higher $^{37}Ar_{Ca}$ signals, reflecting lower chlorine and higher calcium contents dissolved in the PFI fluid. This fact may indicate that the ore-forming fluid had a strong water–rock reaction with the country carbonate rocks resulting in much calcium dissolved. The high potassium in the PFIs is probably correlated with HCO_3^- and CO_3^{2-} dissolved in the ore-forming fluid. The initial $^{40}Ar/^{36}Ar$ value of fluid inclusions can also provide information on fluid origins (Turner and Bannon, 1992; Turner and Wang, 1992). The atmospheric initial $^{40}Ar/^{36}Ar$ ratios of the PFIs may suggest that meteoric water partook in the ore-forming fluids. The obvious excess ^{40}Ar ($^{40}Ar_E$) in the SFIs probably indicates the deep or metamorphic origins, similar to the reports of Turner and Bannon (1992) and Turner and Wang (1992).

5.3. Gas release patterns of hydrothermal minerals by crushing

Gases released by crushing have regular patterns. In this study, the sphalerite gas release patterns have been clearly shown. Now we combine all the data points of the six samples on the Fig. 9 and summarize the following observations:

(1) **K-abundant primary and secondary fluid inclusions** in the cases of 04FK-03Sp and 05Sp (and 04FK-02 & 11, in Qiu and Jiang, 2007) reveal very high $^{40}Ar_{NA}$ (Fig. 9a) and display a very wide range of $^{39}Ar_K/^{40}Ar$ and $^{36}Ar/^{40}Ar$ ratios (Fig. 9b), consistent with well defined PFI isochrons with high-precision ages. SFI isochrons are occasionally obtained.
(2) **K-rich fluid inclusions** in the cases of 04FK-14Sp and 04FK-18Sp are somewhat lower in $^{40}Ar_{NA}$ (Fig. 9a). Again a wide range of $^{39}Ar_K/^{40}Ar$ and $^{36}Ar/^{40}Ar$ ratios (Fig. 9b) produce well-defined PFI isochrons with precise ages. No SFI isochron is obtained.
(3) **K-containing fluid inclusions** in the cases of 04FK-01Sp and 04FK-07Sp are low in $^{40}Ar_{NA}$ (Fig. 9a) and display a narrower range of $^{39}Ar_K/^{40}Ar$ and $^{36}Ar/^{40}Ar$ ratios (Fig. 9b), but still sufficient to define meaningful PFI isochrons.

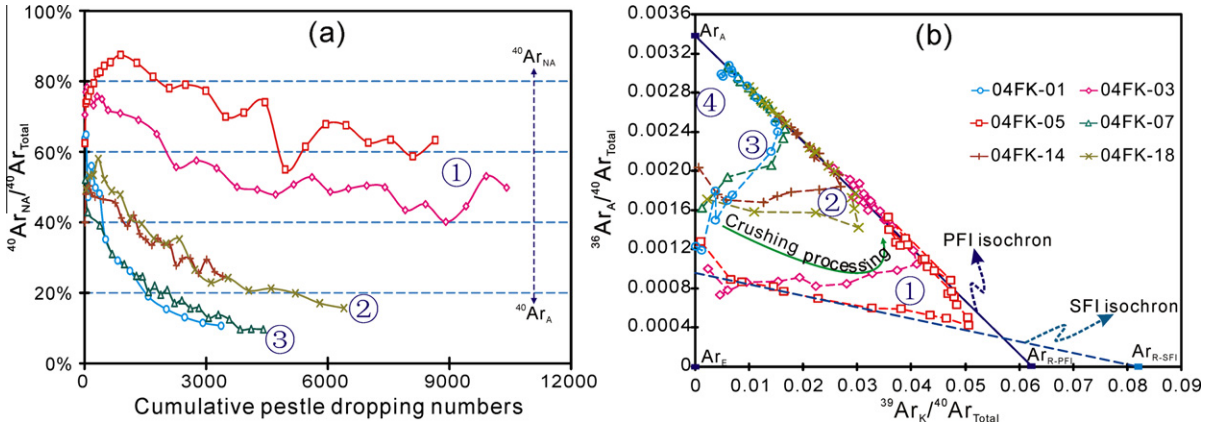

Fig. 9. (a) Release patterns of $^{40}Ar_{NA}$ from crushing as a function of impact events. Higher $^{40}Ar_{NA}$ means more fluid inclusions (both PFIs and SFIs). $^{40}Ar_{NA}$ percentages of all sphalerite samples decrease successively, suggesting that fluid inclusions are gradually exhausted through crushing. (b) Data points of all sphalerites through crushing show similar gas release patterns with a counter-clockwise trend, showing that Ar_E, Ar_R and Ar_A successively contribute to different parts of the degassing. For more information see text.

(4) **K-poor fluid inclusions** were not recognized in this sorts of samples, but would be expected to distribute along the vertical axis because of very low $^{39}Ar_K/^{40}Ar$ ratios and would thus fail to define any isochron.

In general, gas released by crushing is a mixture of Ar_A, Ar_E and Ar_R from both SFIs and PFIs in the early and middle steps, causing data points to spread out in nonlinear arrays. Only in occasional cases with careful crushing extraction may SFI isochrons be obtained for the first few steps. In the late steps, significant isochrons can usually be achieved for samples containing K-bearing PFIs. In order to obtain reliable SFI and PFI isochrons, close attention to the early and late crushing steps is required. Crushing times in the middle steps can be increased significantly to quickly reach the PFIs-dominated degassing steps. In addition, it is very important to crush the samples homogeneously in order to obtain well-defined PFI isochrons.

In summary, the richer the K inside the inclusions, the better the isochron age can be constrained. Based on the results from the present study, it deserves to be mentioned again that the SFI and PFI ages can probably be revealed from the $^{40}Ar_{NA}/^{39}Ar_K$–$^{38}Ar_{Cl}/^{39}Ar_K$ and $^{38}Ar_{Cl}/^{40}Ar_{NA}$–$^{39}Ar_K/^{40}Ar_{NA}$ correlation diagrams (Figs. 5 and 6).

5.4. Significance for the ore genesis

The genesis of Fankou Pb–Zn deposit has been debated for many years because two key elements to understand the ore-forming process – the fluids origin and the mineralization timing – have not been determined. This ore deposit was once considered as a hydrothermal deposit related to a granite intrusion, a sedimentation-subsequent reformation deposit (Lu, 1984) or a sedimentary-accumulative deposit from an ore-bearing hot spring (Chen et al., 1999). Due to lacking suitable minerals for traditional isotopic geochronometers, only a few questionable dates on galena gave Pb model ages of 178, 290 and 398 Ma (Lu, 1984).

The initial $^{40}Ar/^{36}Ar$ ratios of the PFIs obtained in this study clearly suggest the meteoric water origin for the ore-forming fluid. Our new $^{40}Ar/^{39}Ar$ data indicate that the mineralization took place from 300 to 265 Ma (Qiu and Jiang, 2007) in Early to Middle Permian, much later than the Early Carboniferous to Middle Devonian sedimentation ages of the host rocks. Therefore, although the lead and zinc were probably accumulated during the Middle Devonian to Early Carboniferous sedimentation, Early to Middle Permian hydrothermal fluid activities interacting with the sedimentary rocks strongly remobilized and enriched the ore deposit.

6. CONCLUSIONS

This study further investigated the possibility of directly dating the ore mineral sphalerite by $^{40}Ar/^{39}Ar$ progressive crushing technique. The K–Ca–Cl–Ar correlations in the fluid inclusions were discussed in detail in terms of the diagrams based on the $^{40}Ar/^{39}Ar$ results. Some important conclusions are listed as follows:

(1) Sphalerite $^{40}Ar/^{39}Ar$ progressive crushing technique is a promising approach to directly date the ore-forming ages of hydrothermal deposits. The richer the K inside the inclusions, the better the isochron age is constrained.
(2) The SFIs and PFIs are different in volume and have distinctive distribution characteristics leading them to be extracted in the early and later crushing steps, respectively.
(3) On the $^{40}Ar_{NA}/^{39}Ar_K$–$^{38}Ar_{Cl}/^{39}Ar_K$ and $^{38}Ar_{Cl}/^{40}Ar_{NA}$–$^{39}Ar_K/^{40}Ar_{NA}$ correlation diagrams, the data points of SFIs and PFIs distinctly define two groups, indicating that they can be gradually separated by our progressive crushing technique. The ages of SFIs

and PFIs can probably be obtained from these correlation diagrams in addition to the normal and inverse isochron diagrams.

(4) The sphalerite $^{40}Ar/^{39}Ar$ crushing experiments conducted in this and our previous studies indicate sulfide mineralization events took place in the Early and Middle Permian with the participation of meteoric water, and accordingly favor a sedimentation-subsequent reformation ore genesis for the Fankou Pb–Zn deposit.

(5) The progressive crushing technique is very effective at extracting the fluid inclusions within minerals and could be incorporated into the chemical composition and stable isotopic analyses for the fluid inclusions, in order to distinguish the PFIs from the SFIs. We suggest that this technique has a great potential to investigate the genesis of the hydrothermal deposits.

ACKNOWLEDGEMENTS

This research was financially supported by the National Basic Research Program of China (973 Program) (2012CB416706 & 2011CB808906). Prof. A. Kröner is grateful for reading our earlier version of the manuscript. Prof. M. Sun and Dr. G. Zhao are acknowledged for inspiring discussion. We would like to thank Prof. G. Turner for his constructive suggestions that helped greatly improve this paper. We are indebted to Dr. Jan Wijbrans and two anonymous reviewers, as well as associated editor Dr. P.W. Reiners for the constructive reviews and valuable comments that improved the manuscript. Mr. Shuiping Xu and Mr. Shenbo Liu in the Fankou mine are thanked for their helps during the fieldwork. This is contribution No. IS-1455 from the Guangzhou Institute of Geochemistry, Chinese Academy of Sciences (GIGCAS).

APPENDIX A. SUPPLEMENTARY DATA

Here we provide detailed data for sphalerite $^{40}Ar/^{39}Ar$ crushing experiments in Table A1. Supplementary data associated with this article can be found, in the online version, at doi:10.1016/j.gca.2012.01.044.

REFERENCES

Burgess R., Kelley S. P., Parsons I., Walker F. D. L. and Worden R. H. (1992) ^{40}Ar–^{39}Ar analysis of perthite microtextures and fluid inclusions in alkali feldspars from the Klokken syenite, South Greenland. *Earth Planet. Sci. Lett.* **109**, 147–167.

Chen X. M., Zhai Y. S. and Deng J. (1999) Geological and geochemical characteristics of Fankou Pb–Zn Deposit and its metallogenic analysis. *Geol. Geochem.* **27**, 6–14 (In Chinese with English abstract).

Dunlap W. J. and Kronenberg A. K. (2001) Argon loss during deformation of micas: constraints from laboratory deformation experiments. *Contrib. Mineral. Petrol.* **141**, 174–185.

Kelley S., Turner G., Butterfield A. W. and Shepherd T. J. (1986) The source and significance of argon isotopes in fluid inclusion from areas of mineralization. *Earth Planet. Sci. Lett.* **79**, 303–318.

Kendrick M. A., Burgess R., Pattrick R. A. D. and Turner G. (2001) Halogen and Ar–Ar age determinations of inclusions within quartz veins from porphyry copper deposits using complementary noble gas extractions techniques. *Chem. Geol.* **177**, 351–370.

Kendrick M. A., Miller J. M. and Phillps D. (2006a) Part II. Evaluation of ^{40}Ar–^{39}Ar quartz ages: implications for fluid inclusion retentivity and determination of initial $^{40}Ar/^{39}Ar$ values in Proterozoic samples. *Geochim. Cosmochim. Acta* **70**, 2562–2576.

Kendrick M. A., Phillips D. and Miller J. M. (2006b) Part I. Decrepitation and degassing behaviour of quartz up to 1560 °C: analysis of noble gases and halogens in complex fluid inclusion assemblages. *Geochim. Cosmochim. Acta* **70**, 2540–2561.

Kendrick M. A. and Phillips D. (2009) New constraints on the release of noble gases during in vacuo crushing and application to scapolite Br–Cl–I and $^{40}Ar/^{39}Ar$ age determinations. *Geochim. Cosmochim. Acta* **73**, 5673–5692.

Koppers A. A. P. (2002) ArArCALC-software for $^{40}Ar/^{39}Ar$ age calculations. *Comput. Geosci.* **28**, 605–619.

Lu H. (1984) On the genesis of Fankou Pb–Zn ore deposit in Guangdong province. *Geochimica* **13**, 357–365 (In Chinese with English abstract).

Mao J. W., Xie G. Q., Guo C. L. and Chen Y. C. (2007) Large-scale tungsten-tin mineralization in the Nanling region, South China: metallogenic ages and corresponding geodynamic processes. *Acta Petrol. Sin.* **23**, 2329–2338 (In Chinese with English abstract).

Mao J. W., Xie G. Q., Li X. F., Zhang C. Q. and Wang Y. T. (2006) Mesozoic large-scale mineralization and multiple lithospheric extensions in South China. *Acta Geol. Sin. Eng. Ed.* **80**, 420–431.

McKee E. H., Conrad J. E., Turrin B. D. and Theodore T. G. (1993) $^{40}Ar/^{39}Ar$ studies of fluid inclusions in vein quartz from Battle Mountain, Nevada. *US Geol. Surv. Bull.* **2039**, 155–165.

Qiu H. N. (1996) ^{40}Ar–^{39}Ar dating of the quartz samples from two mineral deposits in western Yunnan (SW China) by crushing in vacuum. *Chem. Geol.* **127**, 211–222.

Qiu H. N. and Dai T. M. (1989) $^{40}Ar/^{39}Ar$ technique for dating the fluid inclusions of quartz from a hydrothermal deposit. *Chin. Sci. Bull.* **34**, 1887–1890.

Qiu H. N. and Jiang Y. D. (2007) Sphalerite $^{40}Ar/^{39}Ar$ progressive crushing and stepwise heating techniques. *Earth Planet. Sci. Lett.* **256**, 224–232.

Qiu H. N. and Wijbrans J. R. (2006) Paleozoic ages and excess ^{40}Ar in garnets from the Bixing eclogite in Dabieshan, China: new insights from $^{40}Ar/^{39}Ar$ dating by stepwise crushing. *Geochem. Cosmochim. Acta* **70**, 2354–2370.

Qiu H. N. and Wijbrans J. R. (2008) The Paleozoic metamorphic history of the Central Orogenic Belt of China from $^{40}Ar/^{39}Ar$ geochronology of eclogite fluid inclusions. *Earth Planet. Sci. Lett.* **268**, 501–514.

Qiu H. N., and Wijbrans J. R. (2009) Reply to comment by Kendrick M.A. and Phillips D. (2009) on "The Paleozoic metamorphic history of the Central Orogenic Belt of China from $^{40}Ar/^{39}Ar$ geochronology of eclogite garnet fluid inclusions". *Earth Planet. Sci. Lett.* 279, 395–397.

Qiu H. N., Zhu B. Q. and Sun D. Z. (2002) Age significance interpreted from ^{40}Ar–^{39}Ar dating of quartz samples from the Dongchuan copper deposits, Yunnan, SW China, by crushing and heating. *Geochem. J.* **36**, 475–491.

Renne P. R., Swisher C. C., Deino A. L., Karner D. B., Owens T. L. and DePaolo D. J. (1998) Intercalibration of standards, absolute ages and uncertainties in $^{40}Ar/^{39}Ar$ dating. *Chem. Geol.* **145**, 117–152.

Song X. X. (1984) Minor elements and ore genesis of the Fankou Lead–Zinc deposit. *China Miner. Depos.* **19**, 95–104.

Turner G. (1988) Hydrothermal fluids and argon isotopes in quartz veins and cherts. *Geochem. Cosmochim. Acta* **52**, 1443–1448.

Turner G. and Bannon M. P. (1992) Argon isotope geochemistry of inclusion fluid from granite-associated mineral veins in southwest and northeast England. *Geochimi. Cosmochimi. Acta* **56**, 227–243.

Turner G. and Wang S. S. (1992) Excess argon, crustal fluids and apparent isochrons from crushing K-feldspar. *Earth Planet. Sci. Lett.* **110**, 193–211.

Wijbrans J. R., Pringle M. S., Koppers A. A. P. and Scheveers R. (1995) Argon geochronology of small samples using the Vulkaan argon laser probe. *Proc. K. Ned. Akad. Wet-Biol. Chem. Geol. Phys. Med. Sci.* **98**, 185–218.

Zhang S. G. (2001) Study on the genesis and predication of the metallization of the eastern belt in Fankou lead–zinc deposit, interior report.

Associate editor: Peter Reiners